THE JOURNAL OF PHYSICAL CHEMISTRY C

Article

pubs.acs.org/JPCC

Insight into the Effect of Promoter Mn on Ethanol Formation from Syngas on a Mn-Promoted MnCu(211) Surface: A Comparison with a Cu(211) Surface

Riguang Zhang, Guiru Wang, Baojun Wang,* and Lixia Ling

Key Laboratory of Coal Science and Technology of Ministry of Education and Shanxi Province, Taiyuan University of Technology, Taiyuan 030024, Shanxi, People's Republic of China

Supporting Information

ABSTRACT: Density functional theory calculations have been employed to investigate the effect of promoter Mn on ethanol formation from syngas on a Mn-promoted MnCu(211) surface. Our results show that CO + 3H → CHO + 2H → CH_2O + H → CH_3O is an optimal pathway for the overall CO conversion. Starting with CH_3O, CH_3 is formed via CH_3O → CH_3 + O. Then, CHO insertion into CH_3 can form CH_3CHO, and further, CH_3CHO is successively hydrogenated to ethanol via CH_3CH_2O intermediate. Meanwhile, CH_3OH is formed via CH_3O + H → CH_3OH. Compared to the pure Cu(211) surface, CH_3 formation is found to be energetically compatible with CH_3OH formation on the MnCu(211) surface, which can lead to more CH_3 sources and less CH_3OH; thus, the productivity and selectivity of ethanol can be improved. On the other hand, starting from CH_3, the MnCu(211) surface is more favorable for CHO insertion into CH_3 to CH_3CHO in comparison with CH_3 hydrogenation, dissociation and coupling to CH_4, CH_2, and C_2H_6 due to their high activation barriers; namely, the MnCu(211) surface exhibits a better selectivity toward C_2 oxygenates rather than hydrocarbons. As a result, we can show that, by introducing promoter Mn into Cu catalyst, the productivity and selectivity to ethanol from syngas can be effectively improved.

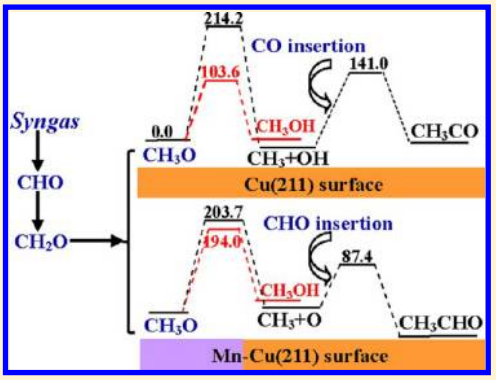

1. INTRODUCTION

Syngas, derived from biomass or coal, has drawn more attention since both sources are abundant, and biomass is a renewable feedstock.[1,2] Among the products from syngas, ethanol is a more desirable product as neat fuels, fuel additives, or a carrier for hydrogen to supply fuel cells and a feedstock for the synthesis of a variety of chemicals, fuels, and polymers.[3−6] Nowadays, many studies have focused on the catalytic conversion of syngas to ethanol; however, no commercial process exists due to the challenging chemical and technological barriers, so low yield and poor selectivity for ethanol formation from syngas remain the major hurdles associated with the use of known catalysts.[7] In order to make this catalytic conversion route commercially attractive, it is essential to develop more effective catalysts.

Among the existing catalysts, Rh is unique for the production of C_2 oxygenates from syngas due to its high selectivity.[8,9] However, considering the high cost and limited availability of Rh, it would be preferable to find some other active catalysts composed of inexpensive metals. Recently, great progress has been made to improve the activity of catalysts composed of inexpensive metals, such as the modified Cu-based catalysts,[10−16] which have been widely used for C_2 oxygenates formation from syngas in the temperature range of 280−310 °C at pressures of about 40−100 bar.[12,16−21]

On the other hand, a large number of works have been performed to investigate the promoting effects of adding promoter metal (Mn, Ce, Ni, Fe, etc.) into supported Rh catalyst to improve the catalytic activity and/or selectivity of ethanol from syngas.[7,22−44] Among these promoters, promoter Mn has been shown to increase the activity and selectivity of C_2 oxygenates from syngas.[36−41] Mei et al.[41] have found that Mn plays an important role in lowering the activation barrier of CO insertion into CH_x (x = 1−3) on Mn-promoted Rh-based/SiO_2 catalyst; thus, the productivity and selectivity to ethanol can be increased. The experimental studies by Luo et al.[42] have further shown that the addition of Mn is essential for the formation of acetic acid and acetaldehyde with high selectivity. Li et al.[43] have found that promoter Mn can improve the selectivity of Rh to convert syngas to ethanol on Mn-promoted Rh-based catalyst. Recently, Ngo et al.[44] have shown that the addition of Mn can improve the selectivity of ethanol on the Fe-promoted Rh/TiO_2 catalysts.

To the best of our knowledge, so far, many investigations about promoters have shown that the additions of promoter into the catalyst can promote the selectivity to ethanol.[10−13,45,46] However, few experimental and theoretical studies have been reported to understand ethanol formation from syngas on Mn-promoted Cu-based catalysts and the effect of promoter Mn on the reaction. Thus, the roles of promoter

Received: September 22, 2013
Revised: February 16, 2014
Published: February 21, 2014

   dx.doi.org/10.1021/jp409447u | J. Phys. Chem. C 2014, 118, 5243−5254

Mn into Cu catalyst and the effect of Mn on ethanol formation from syngas are still unclear; meanwhile, no generally accepted mechanism of ethanol formation from syngas on Mn-promoted MnCu catalyst has been reported.

In the present work, ethanol formation from syngas on the Mn-promoted MnCu(211) surface is systematically investigated with density functional theory (DFT) method together with periodic slab models, aiming to clarify the favorable reaction mechanisms, determine the kinetics, probe into the role of promoter Mn in MnCu catalyst, as well as obtain the effect of Mn on ethanol formation from syngas compared to the reported pure Cu(211) surface.

2. COMPUTATIONAL METHOD

2.1. Computational Method. The DFT calculations are conducted using the code DMol^3 in Materials Studio 5.5.[47,48] The generalized gradient approximation proposed by Perdew and Wang (GGA-PW91)[49,50] is employed for the exchange-correlation functional. An effective core potential (ECP) is used to make the inner electrons of metal atoms frozen and replaced,[51,52] and other atoms are treated with an all-electron basis set. The wave functions are expanded in terms of a double-numerical basis set with a polarization d-function (DNP).[53] Brillouin-zone integrations have been performed using $1 \times 2 \times 1$ k-point grid and a Methfessel-Paxton smearing of 0.005 Ha. In addition, in the discussion of the DFT results, no zero-point energy (ZPE) corrections are included in this study.

The transition state (TS) is located by Complete LST/QST approach.[54] The linear synchronous transit (LST) is conducted to bracket the maximum between the reactants and products, followed by repeated conjugate gradient minimizations and the quadratic synchronous transit (QST) maximizations until a transition state was located.[14,15] In addition, frequency analysis has been used to validate the transition state, and TS confirmation is performed on every transition state to confirm that they lead to the desired reactants and products.[14,15]

2.2. MnCu(211) Surface. There is compelling evidence that stepped surfaces often exhibit a superior catalytic activity over the ideal regular surfaces.[55−62] In fact, the step site is the most common defect for metal catalysts, which may play a key role in catalysis. A stepped (211) surface consists of (111) terrace and the (100)-type step, which can exhibit a better catalytic activity.[61,63−67] For example, Liu et al.[61] have studied NO reduction on Pt-group metals and found that the stepped Ir(211) surface possess high selectivity for NO reduction than that on Ir(111) surface. Xu and Mavrikakis[63] have shown that the adsorption and dissociation of O_2 can be enhanced on the stepped Au(211) surface compared to the flat Au(111) surface. Mavrikakis et al.[66] have found that the stepped Rh(211) surface can lower the activation barrier of CO dissociation by 120 kJ mol^{-1} than the flat Rh(111) surface. Further, Behrens et al.[67] have shown that CO and CO_2 hydrogenation to methanol on the stepped Cu(211) surface exhibits a better catalytic activity than that on the flat Cu(111). Based on the investigations above, the stepped MnCu(211) surface is chosen as the model of Mn-promoted MnCu catalyst to investigate ethanol formation from syngas.

For MnCu(211) surface, two existing forms have been reported: one is that replacing a Cu atom by a Mn atom;[68] the other is that adsorbing a surface Mn atom onto Cu surface.[69−71] As far as we know, for the effect of promoter on C_2 oxygenates formation from syngas, the present studies is mainly focus on the first type of model.[11,14,43,72] Thus, in our study, we only employ the first model via replacing a Cu atom by a Mn atom as the promoter Mn-doped Cu(211) model.

MnCu(211) is modeled using an eight-layer slab model with a 10 Å of vacuum between any two successive slabs. A periodic $p(2 \times 3)$ unit cell is used. During the optimization, the uppermost five layers together with the adsorbates are relaxed, and the bottom three layers are fixed at their bulk positions. For the stepped MnCu(211) surface, three possible sites for Mn atom exist on (211) surface: a step edge, a terrace, or a step base site (see Figure 1). Thus, the most favorable configuration

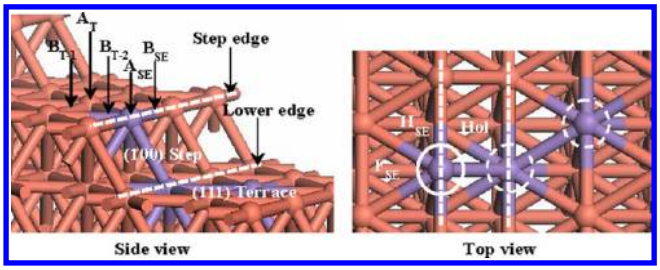

Figure 1. Surface morphology of the MnCu(211) surface with a Mn atom at three different sites marked in a white circle. The purple and orange balls denote Mn and Cu atoms, respectively. A_{SE}, B_{SE}, F_{SE}, and H_{SE} refer to atop, bridge, fcc, and hcp sites on the step edge (SE). F_{LE} and H_{LE} refer to fcc and hcp sites on the lower edge (LE). A_T and B_T refer to atop and bridge sites on the (111) terrace, and Hol refers to the hollow adsorption site on the stepped surface.

of MnCu(211) surface is obtained on the basis of the substitution energy, E_{sub}[14,73,74]

$$E_{sub} = E_{Mn} + E_{Cu(211)} - E_{Cu} - E_{MnCu(211)}$$

where E_{sub} is the substitution energy of MnCu(211) surface and $E_{Cu(211)}$ and $E_{MnCu(211)}$ are the total energies of Cu(211) and MnCu(211) surfaces, respectively. E_{Cu} and E_{Mn} are the total energies of single Cu and Mn atom, respectively. With this definition, the smaller E_{sub} is, the easier the replacement of the Cu atom by a Mn atom.

Our results show that the model with a Mn atom at the step edge is found to be the most easily formed. Among the three sites, as shown in Figure 1, the system, a Cu atom at the step edge replaced by a Mn atom, is chosen to model MnCu(211) surface; there are nine different adsorption sites on the MnCu(211) surface with (111) terrace and (100) step, which are the step edge (atop, bridge, fcc, and hcp), lower edge (fcc and hcp), terrace (atop and bridge), and (100) step (hollow site).[14]

3. RESULTS AND DISCUSSIONS

Nowadays, previous studies have investigated CO hydrogenation reactions without considering the effect of presence of H atom on reaction mechanism,[72,75−77] and the corresponding results can systematically clarify the reaction mechanism, which are consistent with the reported experimental results. On the other hand, in each hydrogenation reaction, although there are a lot of energetically most stable H species on the surface, under a realistic condition, when hydrogenation reaction occurs, only one H adatom interacts with the corresponding adjacent adsorbed species. As a result, we think the effect of the presence of H atoms on reaction mechanism is negligible under a realistic condition, meanwhile, we choose an H atom on the surface to qualitatively investigate CO hydrogenation reaction,

dx.doi.org/10.1021/jp409447u | J. Phys. Chem. C 2014, 118, 5243−5254

and the obtained results are reliable. Therefore, in this study, all the different hydrogenation reaction steps involve the addition of atomic hydrogen present on the surface, only one H atom is presented on the surface for each hydrogenation step involving in ethanol formation from syngas.

3.1. Adsorption of Reactants and Possible Intermediates. For the adsorption of reactants and possible intermediates, all possible adsorption sties on MnCu(211) surface are considered. By our DFT calculations, the most stable configurations of reactants and possible intermediates are presented in Figure 2, and the adsorption energy and key geometrical parameters are shown in Table 1. Our results indicate that all species prefer to interact with the Mn atom rather than the Cu atom after introducing the Mn atom into the Cu catalyst, suggesting that promoter Mn may be the main active site to catalyze ethanol formation from syngas.

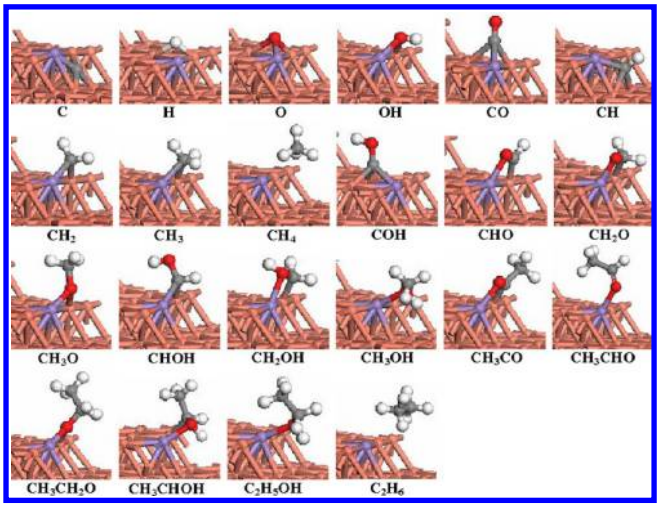

Figure 2. Most stable adsorption configurations of surface species involved in ethanol formation from syngas on MnCu(211). Gray, red, white, orange, and purple balls denote C, O, H, Cu, and Mn atoms, respectively.

Table 1. Adsorption Energy and Key Geometrical Parameters of Reactants, Possible Intermediates and Products Involved in Ethanol Formation from Syngas on MnCu(211) Surface

species	E_{ads} (kJ mol^{-1})	configurations	key parameter (Å)
C	647.8	hollow	Mn−C: 1.881; Cu−C: 1.907, 1.930, 1.933
H	298.7	bridge-T-1	Cu−H: 1.795, 1.700
	298.3	bridge-SE	Mn−H: 1.785, Cu−H: 1.635
O	592.0	hcp-SE	Mn−O: 1.851; Cu−O: 1.919, 2.007
OH	430.9	bridge-SE via O	Mn−O: 1.961; Cu−O: 2.011
CO	154.7	hcp-SE via C	Mn−C: 1.991; Cu−C: 2.121, 2.237
CH	604.2	hollow	Mn−C: 2.009; Cu−C: 2.038, 2.052, 2.073
CH_2	419.1	bridge-SE via C	Mn−C: 1.967; Cu−C: 1.961
CH_3	256.4	bridge-SE via C	Mn−C: 2.156; Cu−C: 2.150
COH	390.5	fcc-SE via C	Mn−C: 1.928; Cu−C: 1.991, 2.000
CHO	263.5	bridge-SE via C and O	Mn−O: 2.077; Cu−C: 1.924
CH_2O	164.5	bridge-SE via C and O	Mn−O: 1.874; C−Cu: 2.123
CH_3O	335.6	bridge-SE via O	Mn−O: 1.946; Cu−O: 2.018
CHOH	321.9	bridge-SE via C	Mn−C: 1.999; Cu−C: 2.041
CH_2OH	244.8	bridge-SE via C and O	Mn−O: 2.134; Cu−C: 1.991
CH_3OH	135.4	atop-SE via O	Mn−O: 2.186
CH_3CO	276.4	bridge-SE via C and O	Mn−O: 2.069; Cu−O: 1.949
CH_3CHO	126.9	atop-SE via O	Mn−O: 2.080
CH_3COH	318.7	bridge-SE via α-C[a]	Mn−C: 2.023; Cu−C: 2.082
CH_3CHOH	222.0	bridge-SE via α-C and O	Mn−O: 2.114; Cu−C: 2.014
C_2H_5OH	124.5	atop-SE via O	Mn−O: 2.063
CH_4	59.7	atop-SE upon Mn	Mn−C: 3.188
C_2H_6	82.1	bridge-SE upon Mn	Mn−C_1: 3.156; Mn−C_2: 3.884

[a] α-C denotes the C atom linked with functional groups.

3.2. Formation Mechanism of CH_x (x = 1−3) Species. *3.2.1. CO Initial Step.* Three reactions may occur for CO initial step involved in ethanol formation from syngas on MnCu(211) surface (R1∼R3). Figure 3 presents the potential energy profile of these reactions together with the structures of initial states (ISs), transition states (TSs), and final states (FSs).

$$CO \rightarrow C + O \quad (R1)$$

$$CO + H \rightarrow COH \quad (R2)$$

$$CO + H \rightarrow CHO \quad (R3)$$

In (R1), the C−O bond cleavage of CO can dissociate into C and O via a transition state TS1. This reaction requires an activation barrier of 392.9 kJ mol^{-1} with the reaction energy of 82.8 kJ mol^{-1}. In TS1, C adsorbs at the Mn−Cu bridge-SE site, and O adsorbs at the Mn atom of step edge. The C−O distance is elongated to 2.076 Å from 1.189 Å in CO.

For (R2), CO hydrogenation to COH via TS2 needs to overcome an activation barrier of 275.9 kJ mol^{-1} with the reaction energy of 83.3 kJ mol^{-1}. In TS2, CO adsorbs at the bridge-T-2 site, and the O−H distance is decreased to 1.597 Å from 4.080 Å in CO + H. In (R3), for CO hydrogenation to CHO via TS3, this reaction is endothermic by 15.8 kJ mol^{-1} and requires an activation barrier of 115.0 kJ mol^{-1}. In TS3, the C−H distance is decreased to 1.432 Å from 3.341 Å in CO+H.

As shown in Figure 3, it can be seen that the direct C−O bond cleavage of CO is very difficult due to the high activation barrier. In contrast, CO hydrogenation to formyl species (COH or CHO) is more plausible, in which CHO formation is more preferred. Thus, the adsorbed CO on MnCu(211) surface is dominantly hydrogenated to CHO.

3.2.2. CH Formation. Above results show that CO hydrogenation to CHO is the main pathway, thus, starting from CHO and CHO+H, only three possible reactions contributes to CH formation (R4∼R6); meanwhile, CHO hydrogenation to CH_2O is also considered (R7). Figure 4 presents the potential energy profile of CH and CH_2O formations, which also includes the structures of ISs, TSs, and FSs.

$$CHO \rightarrow CH + O \quad (R4)$$

dx.doi.org/10.1021/jp409447u | J. Phys. Chem. C 2014, 118, 5243−5254

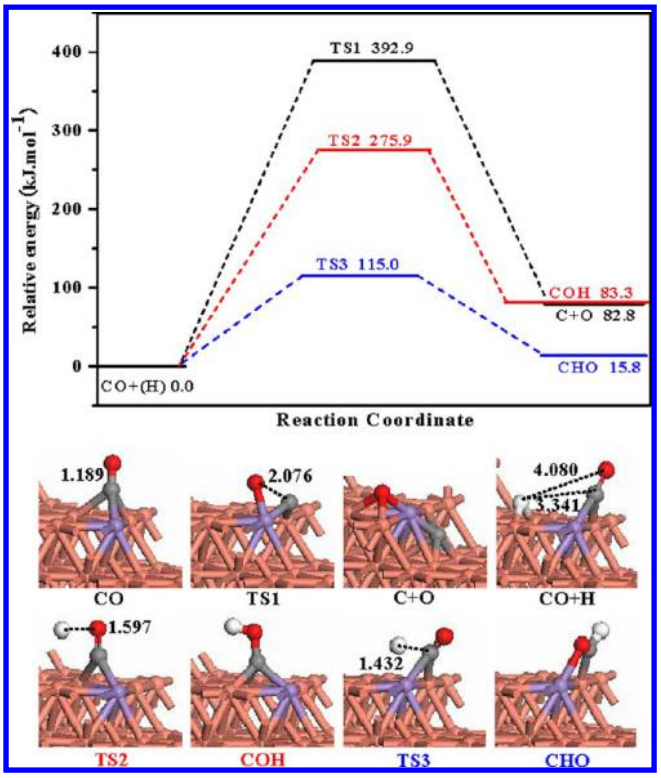

Figure 3. Potential energy profile of CO initial step together with the structures of initial states (ISs), transition states (TSs), and final states (FSs). Bond lengths are in Å. See Figure 2 for color coding.

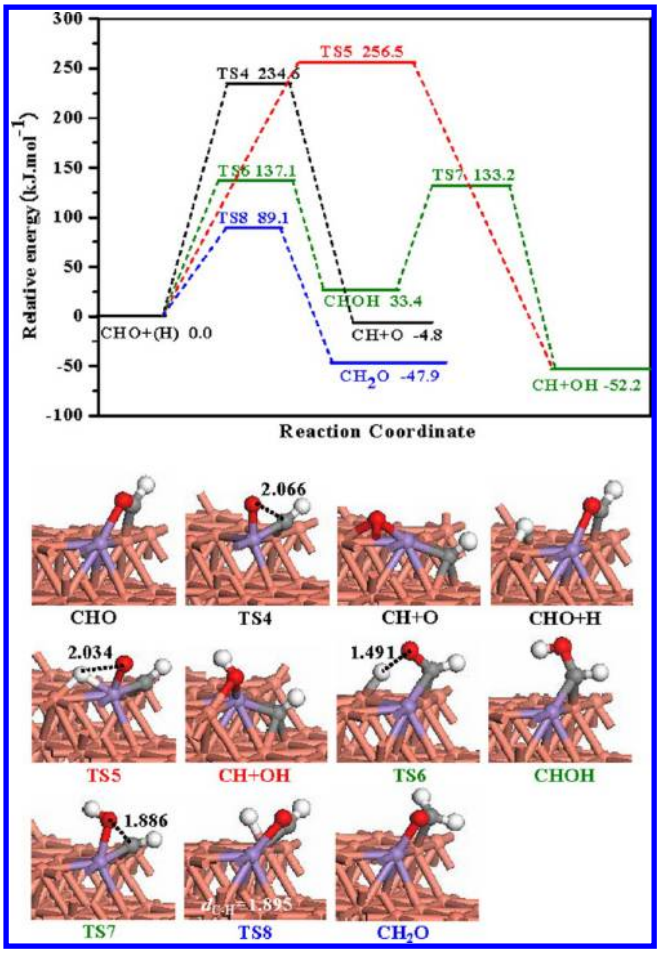

Figure 4. Potential energy profile of CH formation together with the structures of ISs, TSs, and FSs. Bond lengths are in Å. See Figure 2 for color coding.

$$CHO + H \rightarrow CH + OH \quad (R5)$$

$$CHO + H \rightarrow CHOH \rightarrow CH + OH \quad (R6)$$

$$CHO + H \rightarrow CH_2O \quad (R7)$$

For CH formation, in (R4), beginning with the initial state, CHO, the direct dissociation of CHO can form CH and O via TS4, and this reaction is slightly exothermic by 4.8 kJ mol^{-1} with an activation barrier of 234.6 kJ mol^{-1}. In TS4, CH adsorbs at the Mn−Cu bridge-SE site, and O adsorbs at the Mn atom of step edge site. The distance between C and O atoms is 2.066 Å. In (R5), the dissociation of CHO with hydrogen-assisted can form CH + OH via TS5, and this reaction requires an activation barrier of 256.5 kJ mol^{-1}. It is exothermic by 52.2 kJ mol^{-1}. In TS5, CH adsorbs at the Mn−Cu bridge-SE site, O adsorbs at the Mn atom of step edge, and H adsorbs at the bridge-T-2 site. In (R6), H adatom first associates with the O atom of CHO via TS6 to form CHOH, and this reaction is endothermic by 33.4 kJ mol^{-1} with an activation barrier of 137.1 kJ mol^{-1}. In TS6, CHO adsorbs at the Mn−Cu bridge-SE site via C atom and H adsorbs at the atop-T site. Subsequently, CHOH further dissociates into CH + OH via TS7 with an activation barrier of 99.8 kJ mol^{-1}, and this reaction is exothermic by 85.6 kJ mol^{-1}. In TS7, CH adsorbs at the Mn−Cu bridge-SE site, and OH adsorbs at the Mn atom of step edge; the distance between C and O atoms is 1.886 Å.

For (R7), starting from CHO + H, CHO can be hydrogenated to CH_2O via TS8 with an activation barrier of 89.1 kJ mol^{-1}, this reaction is exothermic by 47.9 kJ mol^{-1}. In TS8, CHO adsorbs at the Mn−Cu bridge-SE site via both C and O atoms, and H adsorbs at the Cu atom of step edge.

As shown in Figure 4, for CH formation (R4−R6), starting with CHO or CHO + H, (R6) dominantly contributes to CH formation via CHOH intermediate in kinetics, which has the highest barrier of 137.1 kJ mol^{-1} with the reaction energy of −52.2 kJ mol^{-1} shown as the green line. However, CHO hydrogenation to CH_2O (R7) has only the highest barrier and reaction energy of +89.1 and −47.9 kJ mol^{-1} shown as the blue line, respectively. As a result, CHO can be more easily hydrogenated to CH_2O rather than CHOH and CH by CHOH dissociation.

3.2.3. CH_2 Formation. Similarly, CHO is dominantly hydrogenated to CH_2O on MnCu(211) surface, and as a result, CH_2O dissociation and hydrogenation are further investigated: Four reactions are responsible for CH_2 formation (R8−R11), in which R9 starts with CHO + H; meanwhile, CH_2O hydrogenation to CH_3O is also considered (R12). Figure 5 presents the potential energy profile of CH_2 and CH_3O formations together with the structures of ISs, TSs, and FSs.

$$CH_2O \rightarrow CH_2 + O \quad (R8)$$

$$CHO + H \rightarrow CH_2 + O \quad (R9)$$

$$CH_2O + H \rightarrow CH_2 + OH \quad (R10)$$

$$CH_2O + H \rightarrow CH_2OH \rightarrow CH_2 + OH \quad (R11)$$

$$CH_2O + H \rightarrow CH_3O \quad (R12)$$

dx.doi.org/10.1021/jp409447u | J. Phys. Chem. C 2014, 118, 5243−5254

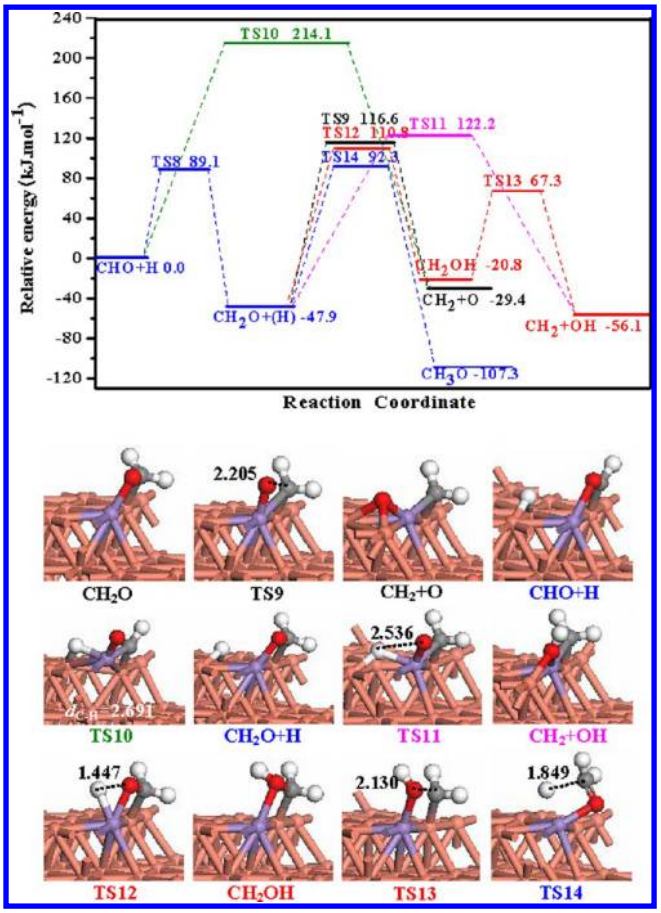

Figure 5. Potential energy profile of CH_2 formation together with the structures of ISs, TSs, and FSs. Bond lengths are in Å. See Figure 2 for color coding.

For CH_2 formation, in (R8), the direct dissociation of CH_2O via TS9 is endothermic by 18.5 kJ mol^{-1} with an activation barrier of 164.5 kJ mol^{-1}. In TS9, CH_2 adsorbs at the Mn−Cu bridge-SE site, and O adsorbs at the Mn atom of step edge. The distance between C and O atoms is 2.205 Å. In (R9), CHO dissociation with hydrogen-assisted to CH_2 + O via TS10 requires an activation barrier of 214.1 kJ mol^{-1}, and it is exothermic by 29.4 kJ mol^{-1}. In TS10, CH adsorbs at the Mn−Cu bridge-SE site, O adsorbs at the Mn atom of step edge, and H adsorbs at the bridge-T-2 site. In (R10), the dissociation of CH_2O with hydrogen-assisted can form CH_2 + OH via TS11. This reaction needs an activation barrier of 170.1 kJ mol^{-1}, and it is slightly exothermic by 8.2 kJ mol^{-1}. In TS11, CH_2 adsorbs at the Mn−Cu bridge-SE site, O adsorbs at the Mn atom of step edge, and H adsorbs at the bridge-T-2 site. In (R11), CH_2O is first hydrogenated to CH_2OH via TS12, and this reaction is endothermic by 27.1 kJ mol^{-1} with an activation barrier of 158.7 kJ mol^{-1}. In TS12, CH_2O adsorbs at the Mn−Cu bridge-SE site via both C and O atoms, and H adsorbs at the Mn atom of step edge; subsequently, CH_2OH further dissociates into CH_2 + OH via TS13 with an activation barrier of 88.1 kJ mol^{-1}, and it is exothermic by 35.3 kJ mol^{-1}. In TS13, OH adsorbs at the Mn atom of step edge, and CH_2 adsorbs at the Cu atom of step edge.

In (R12), CH_2O hydrogenation to CH_3O via TS14 is exothermic by 59.4 kJ mol^{-1} with an activation barrier of 140.2 kJ mol^{-1}. In TS14, CH_2O adsorbs at the Mn atom of step edge via O atom.

We can obtain from Figure 5 that among four reactions of CH_2 formation (R8−R11), starting with CHO + H, (R11) dominantly contributes to CH_2 formation via CH_2OH intermediate in kinetics, which has the highest barrier of 110.8 kJ mol^{-1} with the reaction energy of −56.1 kJ mol^{-1} in a red line. However, CH_2O hydrogenation to CH_3O (R12) has only the highest barrier and reaction energy of 92.3 and −107.3 kJ mol^{-1} in a blue line, respectively. Thus, the intermediate CH_2O can be more easily hydrogenated to CH_3O rather than CH_2OH and CH_2 by CH_2OH dissociation.

3.2.4. CH_3 Formation. As mentioned above, CH_2O is dominantly hydrogenated to CH_3O, and as a result, CH_3O dissociation and hydrogenation reactions are further examined. Three reactions are responsible for CH_3 formation (R13∼R15), in which R13 begins with CH_2O + H. Meanwhile, CH_3O hydrogenation to CH_3OH (R16) has been considered. Figure 6 presents the potential energy profile of CH_3 and CH_3OH formations together with the structures of ISs, TSs, and FSs.

$$CH_2O + H \rightarrow CH_3 + O \quad \text{(R13)}$$

$$CH_3O \rightarrow CH_3 + O \quad \text{(R14)}$$

$$CH_3O + H \rightarrow CH_3 + OH \quad \text{(R15)}$$

$$CH_3O + H \rightarrow CH_3OH \quad \text{(R16)}$$

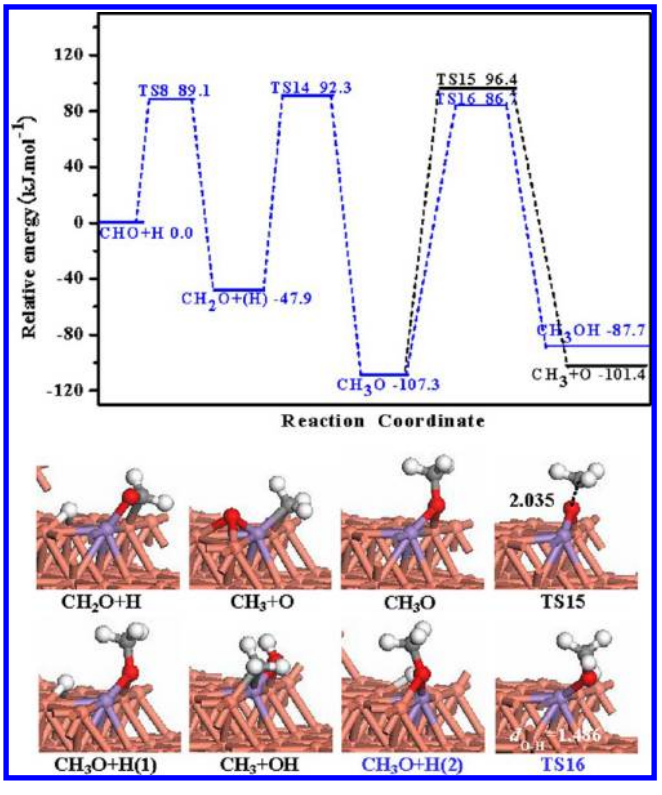

Figure 6. Potential energy profile of CH_3 formation together with the structures of ISs, TSs, and FSs. Bond lengths are in Å. See Figure 2 for color coding.

For CH_3 formation, in (R13), CH_2O dissociation with hydrogen-assisted leads to CH_3 + O, our result obtained by TS confirmation shows that CH_2O dissociation with hydrogen-assisted prefers to form CH_2 + O + H rather than CH_3 + O. In (R14), the direct dissociation of CH_3O tends to produce CH_3 + O via TS15. This reaction requires an activation barrier of

dx.doi.org/10.1021/jp409447u | J. Phys. Chem. C 2014, 118, 5243−5254

203.7 kJ mol^{-1}, and it is slightly endothermic by 5.8 kJ mol^{-1}. In TS15, O adsorbs at the Mn−Cu bridge-SE site, CH_3 is away from the surface, and the distance between C and O atoms is 2.035 Å. In (R15), for CH_3O dissociation with hydrogen-assisted into CH_3 + OH, similarly, our result obtained by TS confirmation shows that this reaction prefers to form CH_3 + O + H rather than CH_3 + OH. For CH_3O hydrogenation to CH_3OH in (R16) via TS16, this reaction requires an activation barrier of 194.0 kJ mol^{-1}, and it is endothermic by 19.6 kJ mol^{-1}. In TS16, CH_3O adsorbs at the Mn atom of step edge.

It can be seen from Figure 6 that among all reactions of CH_3 formation (R13∼R15), starting from CHO + H, (R14) is the most favorable pathway in kinetics, which is also the only pathway for CH_3 formation via the direct dissociation of CH_3O. This reaction shown as a black line has the highest barrier of 96.4 kJ mol^{-1} with the reaction energy of −101.4 kJ mol^{-1}. Meanwhile, CH_3O hydrogenation to CH_3OH (R16) shown as a blue line has the highest barrier 92.3 kJ mol^{-1} with the reaction energy of −87.7 kJ mol^{-1}. The highest barriers of CH_3 and CH_3OH formations differ only by 4.1 kJ mol^{-1}, indicating that CH_3 formation is energetically compatible with CH_3OH formation on MnCu(211) surface.

3.3. Comparisons for CH_x (x = 1−3) and CH_3OH Formations. With respect to CHO + H, the potential energy profile for the most favorable pathway of CH_x (x = 1−3) and CH_3OH formations is summarized in Figure 7. CH formation

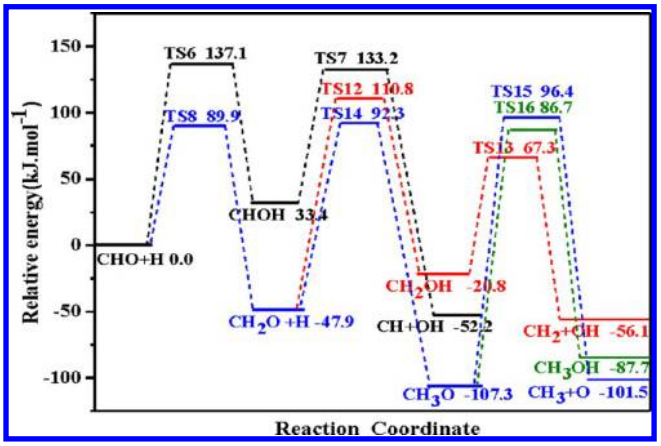

Figure 7. Potential energy profile for the most favorable pathway of CH_x (x = 1−3) and CH_3OH formations with respect to CHO + H.

shown as a black line has the highest barrier and reaction energy of +137.1 and −52.2 kJ mol^{-1}. CH_2 formation shown as a red line has the highest barrier and reaction energy of +110.8 and −56.1 kJ mol^{-1}. CH_3 formation shown as a blue line has the highest barrier and reaction energy of +96.4 and −101.4 kJ mol^{-1}. Thus, CH_3 is more easily formed both thermodynamically and dynamically than CH and CH_2 species, namely among all CH_x (x = 1−3) species, CH_3 is the most favorable monomer via the reaction process of CO + 3H → CHO + 2H → CH_2O + H → CH_3O → CH_3 + O (R3), (R7), (R12), and (R14), the corresponding rate-limiting step occurs at (R14) with an activation barrier of 203.7 kJ mol^{-1}. Meanwhile, CH_3OH formation in a green line has the highest barrier and reaction energy of +92.3 and −87.7 kJ mol^{-1}, which is formed by CO + 4H → CHO + 3H → CH_2O + 2H → CH_3O + H → CH_3OH (R3), (R7), (R12), and (R16), the corresponding rate-limiting step occurs at (R16) with an activation barrier 194.0 kJ mol^{-1}.

On the basis of the above results, we can obtain CO + 3H → CHO + 2H → CH_2O + H → CH_3O (R3), (R7), and (R12) as the common steps for the initial CO hydrogenation on MnCu(211) surface; starting from CH_3O, CH_3O dissociation to CH_3 is energetically compatible with CH_3O hydrogenation to CH_3OH due to the small difference for the activation barrier of the rate-limiting step by 9.7 kJ mol^{-1}. Our results on the MnCu(211) surface are quite different from those obtained on the pure Cu(211) surface.[14]

3.4. C_2H_5OH and Byproducts Formations. *3.4.1. CH_3 Hydrogenation, Dissociation, Coupling, and CO/CHO Insertion into CH_3.* C_2 oxygenate formations on Rh-based[72,75,78] and Cu-based catalysts[14,15] have shown that CH_3 species will undergo four types of reactions, CH_3 hydrogenation to CH_4, CH_3 coupling to C_2H_6, CO/CHO insertion into CH_3 to C_2 oxygenates, and CH_3 dissociation into CH_2 + H. As a result, five possible reactions (R17−R21) are investigated. Figure 8 presents the potential energy profile of these reactions together with the structures of ISs, TSs, and FSs.

$$CH_3 + H \rightarrow CH_4 \quad \text{(R17)}$$

$$CH_3 \rightarrow CH_2 + H \quad \text{(R18)}$$

$$CH_3 + CH_3 \rightarrow C_2H_6 \quad \text{(R19)}$$

$$CH_3 + CO \rightarrow CH_3CO \quad \text{(R20)}$$

$$CH_3 + CHO \rightarrow CH_3CHO \quad \text{(R21)}$$

In (R17), CH_3 hydrogenation to CH_4 via TS17 is exothermic by 21.9 kJ mol^{-1}, and it has an activation barrier of 129.0 kJ mol^{-1}. In TS17, both CH_3 and H adsorb at the Mn atom of step edge. In (R18), CH_3 dissociation into CH_2 + H via TS18 requires an activation barrier of 135.7 kJ mol^{-1}, and it is endothermic by 76.0 kJ mol^{-1}. In TS18, CH_2 adsorbs at the Mn−Cu bridge-SE site and H adsorbs at the Mn atom of step edge. In (R19), CH_3 coupling to C_2H_6 via TS19 has an activation barrier of 211.0 kJ mol^{-1}, and it is exothermic by 37.7 kJ mol^{-1}. In TS19, one CH_3 adsorbs at the Mn atom of step edge via C atom, and the other is away from the surface with the C−C bond length of 2.185 Å. In (R20), CO insertion into CH_3 to CH_3CO via TS20 has an activation barrier of 173.1 kJ mol^{-1} with the reaction energy of −16.4 kJ mol^{-1}. In TS20, CO adsorbs at the Mn atom of step edge with the C−C bond length of 2.212 Å. In (R21), CHO insertion into CH_3 first forms the intermediate IM via TS21, this reaction is endothermic by 21.3 kJ mol^{-1} with an activation barrier of 39.5 kJ mol^{-1}. In TS21, CHO adsorbs at the Cu atom of step edge via C atom, and CH_3 adsorbs at the Mn−Cu bridge-SE site with the C−C bond length of 3.611 Å. Subsequently, IM further forms CH_3CHO via TS22, and this reaction is exothermic by 86.2 kJ mol^{-1} with an activation barrier of 66.1 kJ mol^{-1}. In TS22, CHO adsorbs at the Mn−Cu bridge-SE site, and CH_3 adsorbs at the Mn atom of step edge with the C−C bond length of 1.886 Å.

It can be seen from Figure 8 that starting from CH_3 species, CH_3 hydrogenation, dissociation, coupling, and CO insertion into CH_3 are more difficult to occur because of the high activation barrier, whereas, CHO insertion into CH_3 to CH_3CHO is the most favorable, which dominantly contributes to C_2 oxygenates formation of ethanol precursor. Meanwhile, it is noted that when CHO insertion into CH_3 occurs, CHO can also be hydrogenated to CH_2O with the activation barrier and reaction energy of 89.1 and −47.9 kJ mol^{-1}, respectively, which

dx.doi.org/10.1021/jp409447u | J. Phys. Chem. C 2014, 118, 5243−5254

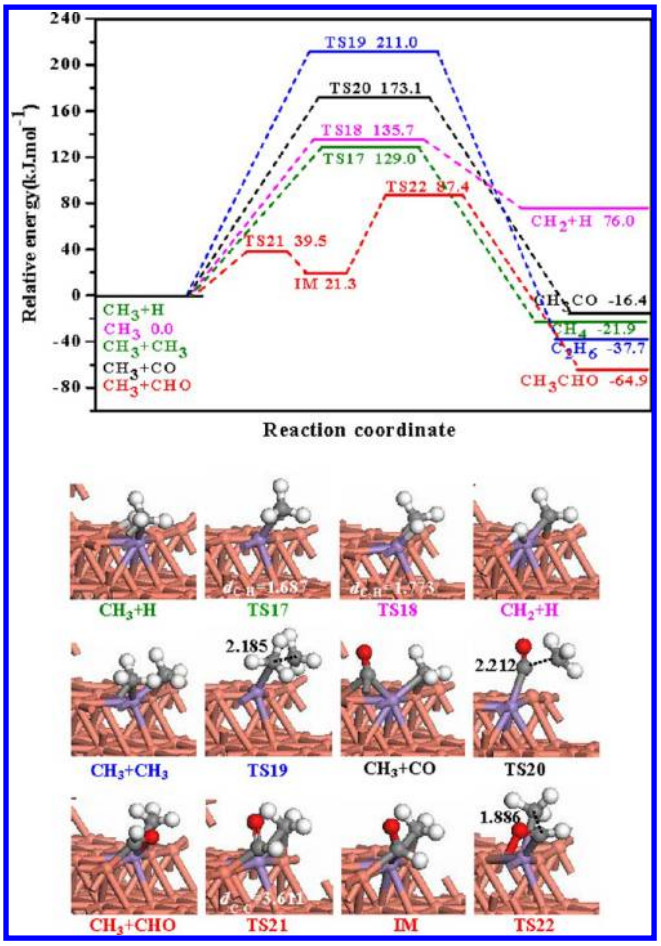

Figure 8. Potential energy profile of CH_4, CH_2, C_2H_6, CH_3CO, and CH_3CHO formations starting from CH_3 together with the structures of ISs, TSs, and FSs. Bond lengths are in Å. See Figure 2 for color coding.

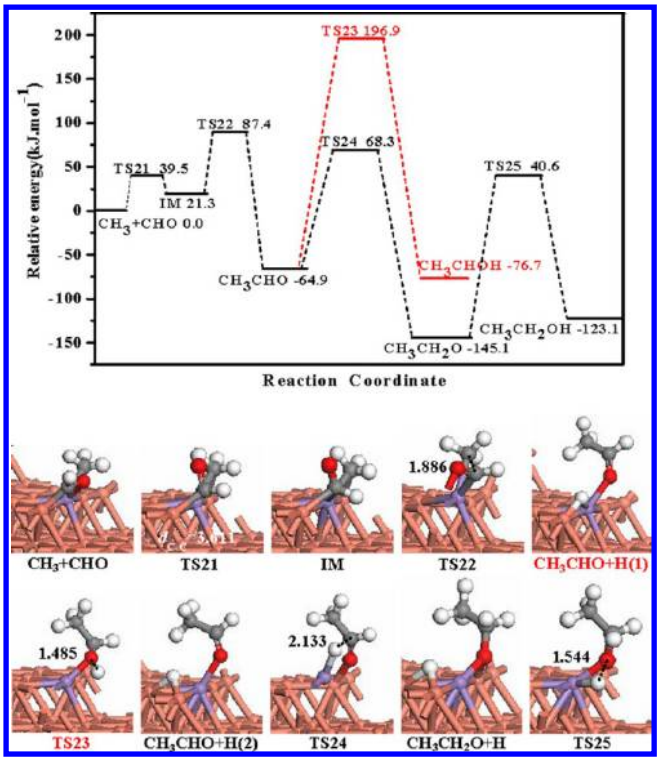

Figure 9. Potential energy profile of CHO insertion into CH_3 to CH_3CHO and further hydrogenation to ethanol together with the structures of ISs, TSs, and FSs. Bond lengths are in Å. See Figure 2 for color coding.

is energetically compatible with CHO insertion into CH_3 to CH_3CHO; thus, partial CHO involves in hydrogenation to CH_2O, and the rest inserts into CH_3 to CH_3CHO. Interestingly, previous studies on the pure Cu(211) surface have shown that CHO hydrogenation to CH_2O is more preferable than CH_3CHO formation via CHO insertion into CH_3.[14]

3.4.2. CH_3CHO Hydrogenation to Ethanol on MnCu(211) Surface. As mentioned above, C_2 oxygenates of ethanol precursor are mainly formed by CHO insertion into CH_3, and C_2H_5OH are formed by CH_3CHO hydrogenation, in which two possible pathways exist, one is atomic H interacting with α-C atom of CH_3CHO to CH_3CH_2O, and the other is atomic H associating with O atom of CH_3CHO to CH_3CHOH. Figure 9 presents the potential energy profile of these reactions together with the structures of ISs, TSs, and FSs.

$$CH_3CHO + H \rightarrow CH_3CHOH \quad (R22)$$

$$CH_3CHO + H \rightarrow CH_3CH_2O \quad (R23)$$

$$CH_3CH_2O + H \rightarrow C_2H_5OH \quad (R24)$$

In R22, CH_3CHO hydrogenation to CH_3CHOH via TS23 is exothermic by 11.8 kJ mol^{-1} with an activation barrier of 261.8 kJ mol^{-1}. In TS23, CH_3CHO adsorbs at the Mn atom of step edge. In R23, CH_3CHO hydrogenation to CH_3CH_2O via TS24 is exothermic by 80.2 kJ mol^{-1} with an activation barrier of 133.2 kJ mol^{-1}. In TS24, CH_3CHO adsorbs at the Cu atom of step edge, and H adsorbs at the Mn atom of step edge. As a result, CH_3CHO is mainly hydrogenated to CH_3CH_2O, followed by its hydrogenation to ethanol via TS25. This reaction is endothermic by 22.0 kJ mol^{-1} with an activation barrier of 185.7 kJ mol^{-1}. In TS25, both CH_3CH_2O and H adsorb at the Mn atom of step edge.

3.5. Brief Summary of Ethanol Formation. Above DFT results show that CO + 3H → CHO + 2H → CH_2O + H → CH_3O (R3), (R7), and (R12) is an optimal pathway for the initial CO hydrogenation on MnCu(211) surface. Starting with CH_3O, ethanol formation first goes through CH_3O dissociation to produce CH_3, subsequently, CHO inserts into CH_3 to form CH_3CHO, and further CH_3CHO is successively hydrogenated to ethanol. CH_3 formation by direct CH_3O dissociation is the rate-limiting step of ethanol formation with the activation barrier and reaction energy of 203.7 and 5.8 kJ mol^{-1}, respectively. Meanwhile, CHO insertion into CH_3 to CH_3CHO is also a key step for the formation of ethanol precursor. Further, starting from CH_3, since CHO insertion into CH_3 to CH_3CHO is the most favorable pathway among all reactions related to CH_3 species, and the MnCu(211) surface exhibits a better selectivity to C_2 oxygenates rather than hydrocarbons. On the other hand, CH_3OH is formed by CH_3O hydrogenation to CH_3OH, which is the rate-limiting step of CH_3OH formation with the activation barrier and reaction energy of 194.0 and 19.6 kJ mol^{-1}, respectively. More importantly, CH_3 formation via direct CH_3O dissociation is energetically compatible with CH_3OH formation via CH_3O hydrogenation.

dx.doi.org/10.1021/jp409447u | J. Phys. Chem. C 2014, 118, 5243−5254

For most of elementary reactions involved in ethanol formation, the step sites around the Mn atom of the MnCu(211) surface are the active centers, and this result is consistent with the properties of the (211) surface containing steps, which exhibits good catalytic performance in catalytic reactions.[62,64,75] As a result, the step sites around the Mn atom of the MnCu(211) surface play an important role in promoting ethanol formation from syngas.

3.6. Comparisons for Ethanol Formation Between MnCu(211) and Cu(211) Surfaces. It has been well accepted that CH_x and C_2 oxygenates are the two crucial steps for ethanol formation from syngas.[31,41,43,72,79] Our results also show that CH_3 and CH_3CHO on MnCu(211) surface are two crucial steps. In order to probe into the roles of promoter Mn and its effect on ethanol formation from syngas over Cu-based catalysts, we further compare these two key steps between MnCu(211) and Cu(211) surfaces.[14]

3.6.1. CH_3 and CH_3OH Formation. Our previous results on Cu(211) surface have shown that the initial CO hydrogenation is via an optimal pathway of CO + 3H → CHO + 2H → CH_2O + H → CH_3O,[14] which is consistent with those on MnCu(211) surface. Starting from CH_3O, Figure 10 presents the potential

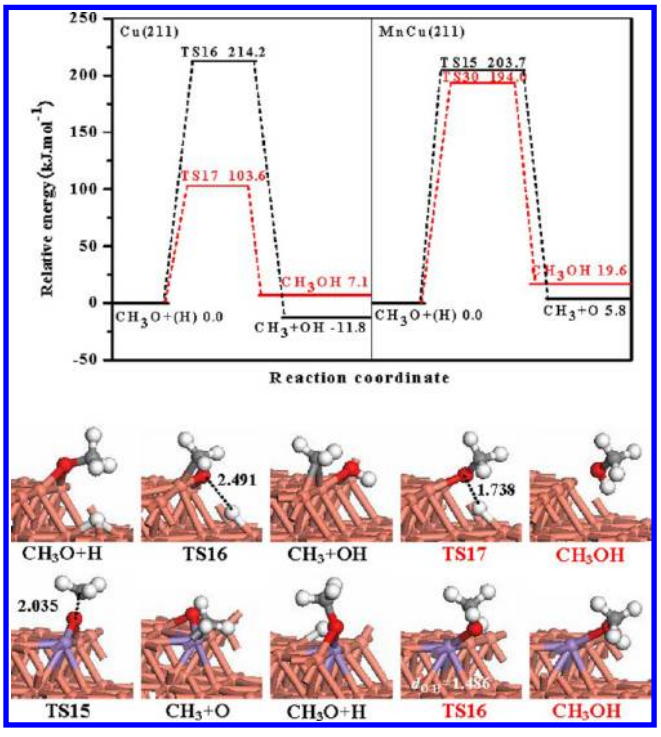

Figure 10. Potential energy profile of CH_3 and CH_3OH formations starting from CH_3O on Cu(211) and RhCu(211) surfaces together with the structures of ISs, TSs, and FSs. Bond lengths are in Å. See Figure 2 for color coding.

energy profile of CH_3 and CH_3OH formations on both Cu(211) and MnCu(211) surfaces, respectively. First, CH_3 is mainly formed via CH_3O + H → CH_3 + OH on Cu(211), while CH_3 is mainly formed via CH_3O → CH_3 + O on MnCu(211). Second, the activation barriers of CH_3 and CH_3OH formation on Cu(211) differ largely by 110.6 kJ mol^{-1}, indicating that CH_3O hydrogenation to CH_3OH is superior to CH_3O dissociation to CH_3 on Cu(211), whereas the corresponding difference values of activation barriers on MnCu(211) is only 9.7 kJ mol^{-1}, suggesting that CH_3O dissociation to CH_3 is energetically compatible with CH_3O hydrogenation to CH_3OH on MnCu(211). Third, the activation barrier of CH_3 formation on MnCu(211) is lower by 10.5 kJ mol^{-1} than that on Cu(211), namely, CH_3 formation is more preferred in kinetics on MnCu(211) surface. Finally, the activation barrier of CH_3OH formation on MnCu(211) is significantly higher by 90.4 kJ mol^{-1} than that on Cu(211), indicating that CH_3OH formation on MnCu(211) can be suppressed compared with that on Cu(211).

The above results show that, after introducing Mn promoter into Cu catalyst, the MnCu(211) surface presents a new reaction pathway of CH_3 formation, CH_3 sources can be significantly increased, and CH_3OH formation can be significantly decreased. As a result, more CH_3 can involve in ethanol formation from syngas, and the productivity and selectivity of ethanol can be effectively improved.

3.6.2. C_2 Oxygenates of Ethanol Precursor. As shown in Figure 11, on Cu(211) surface,[14] CO insertion into CH_3 to

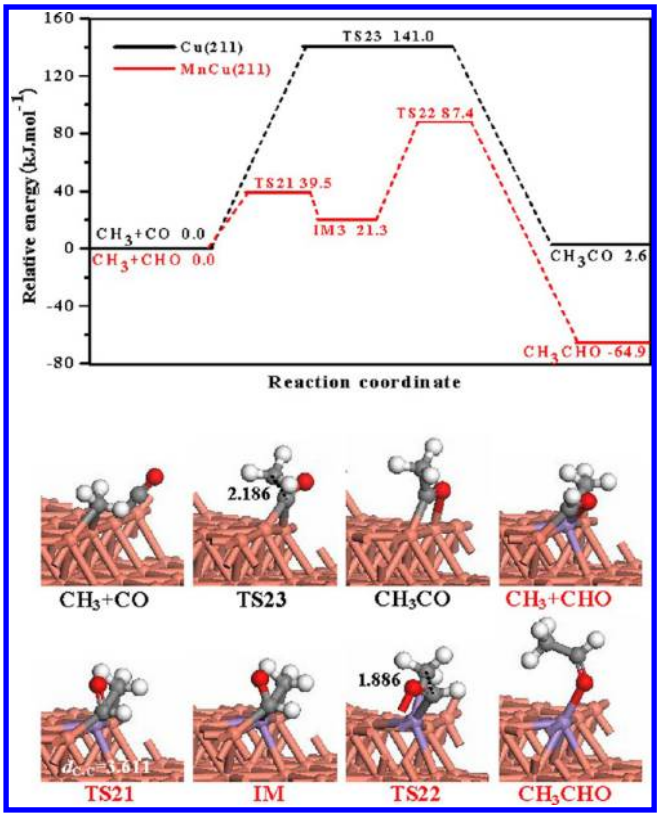

Figure 11. Potential energy profiles of CHO insertion into CH_3 to CH_3CHO on Cu(211) and CO insertion into CH_3 to CH_3CO on MnCu(211) together with the structures of ISs, TSs, and FSs. Bond lengths are in Å. See Figure 2 for color coding.

CH_3CO mainly contributes to C_2 oxygenates formation of ethanol precursor, the highest barrier and reaction energy shown as a black line are 141.0 and 2.6 kJ mol^{-1}, respectively, while on MnCu(211) surface, CHO insertion into CH_3 to CH_3CHO mainly contributes to C_2 oxygenates formation, the highest barrier and reaction energy shown as a red line are +87.4 and −64.9 kJ mol^{-1}, respectively; thus, C_2 oxygenates formation of ethanol precursor is more easily formed in kinetics and thermodynamics on MnCu(211) than that on Cu(211).

On the other hand, according to the Eyring's transition state theory (TST),[14] we have further calculated the rate constants of

dx.doi.org/10.1021/jp409447u | J. Phys. Chem. C 2014, 118, 5243−5254

these key steps at different temperatures on Cu(211) and MnCu(211) surfaces, respectively; the rate constant are obtained as the following formula:

$$k = \frac{k_b T}{h}\left(\frac{p^0}{RT}\right)^{1-n} \exp\left[-\frac{\Delta_r G_m^{\ddagger}}{RT}\right]$$

where T is the reaction temperature, k is the rate constant, k_b, h, p^0, and R are Boltzmann's constant, Planck's constant, standard atmospheric pressure, and the fundamental gas constant, respectively, and n is the number of reactants.

Previous studies have reported that Cu-based catalysts exhibit a good catalytic activity to C_2 oxygenates formation from syngas, where the reaction temperature ranges from 553 to 583 K.[12,14,80−82] Therefore, the rate constants of C_2 oxygenates formation at T = 550, 575, and 600 K have been calculated, respectively, as listed in Table 2.

Table 2. Rate Constant k for the Elementary Reactions of Ethanol Precursor Formation on Cu(211) and MnCu(211) Surfaces at the Different Temperatures

		rate constant k/s^{-1}		
	elementary reaction	550 K	575 K	600 K
Cu(211)	$CH_3 + CO \rightarrow CH_3CO$	7.98	31.76	112.79
MnCu(211)	$CH_3 + CHO \rightarrow CH_3CHO$	6.91×10^4	1.67×10^5	3.77×10^5

It can be obtained from Table 2 that the rate constant k of C_2 oxygenates formation increases with the increase of temperature on both Cu(211) and MnCu(211) surfaces. Meanwhile, at the same temperature, the rate constant of CH_3CHO formation on MnCu(211) is much larger than that of CH_3CO formation on Cu (211), which means that CH_3CHO formation on MnCu(211) is much easier than CH_3CO formation on Cu(211). Thus, compared to the pure Cu(211), Mn-promoted MnCu(211) can facilitate C_2 oxygenates formation, and enhance the productivity and selectivity to ethanol from syngas.

Above results mean that introducing promoter Mn into Cu catalyst not only leads to a new formation pathway of C_2 oxygenates but also promotes C_2 oxygenates formation, and as a result, the productivity and selectivity to ethanol from syngas can be improved.

3.7. Comparisons for Ethanol Formation Between MnCu(211) and Rh Surfaces. Nowadays, Rh-based catalysts have been used in catalyzing ethanol formation from syngas due to the unique efficiency and selectivity; thus, previous DFT studies on Rh catalyst obtained by Choi and Liu[72] as well as Kapur et al.[75] have been compared with our present results on MnCu catalyst. Table 3 lists the corresponding activation barrier and reaction energy of the key steps.

First, $CO + 3H \rightarrow CHO + 2H \rightarrow CH_2O + H \rightarrow CH_3O$ is the common optimal pathway on MnCu and Rh surfaces;[75] Beginning with CH_3O, on Rh(111) and Rh(211) surfaces, the differences of activation barrier between CH_3 and CH_3OH formations are 51.2 and 19.3 kJ mol^{-1}, respectively; whereas, on the MnCu(211) surface, the differences are only 9.7 kJ mol^{-1}; thus, compared to Rh catalyst, CH_3 formation is energetically compatible with CH_3OH formation, namely, more CH_3 sources can be obtained to participate the C_2 oxygenates formation.

Table 3. Activation Barriers and Reaction Energies of the Reactions for CO Insertion into CH_3 and CH_3 Hydrogenation to CH_4, as Well as CH_3 and CH_3OH Formations on Cu and Rh Surfaces

surface	elementary reaction	E_a/kJ mol^{-1}	ΔH/kJ mol^{-1}
MnCu(211)	$CH_3 + CHO \rightarrow CH_3CHO$	87.4	−64.9
	$CH_3 + H \rightarrow CH_4$	129.0	−21.9
	$CH_3O + H \rightarrow CH_3 + OH$	203.7	5.8
	$CH_3O + H \rightarrow CH_3OH$	194.0	19.6
Rh(111)[a]	$CH_3 + CO \rightarrow CH_3CO$	89.7	14.5
	$CH_3 + H \rightarrow CH_4$	55.0	−19.3
	$CH_3O \rightarrow CH_3 + O$	102.3	−18.3
	$CH_3O + H \rightarrow CH_3OH$	88.8	3.9
Rh(111)[b]	$CH_3 + CO \rightarrow CH_3CO$	126.4	11.6
	$CH_3O \rightarrow CH_3 + O$	97.5	78.2
	$CH_3O + H \rightarrow CH_3OH$	46.3	−28.9
Rh(211)[b]	$CH_3 + CO \rightarrow CH_3CO$	129.3	38.6
	$CH_3O \rightarrow CH_3 + O$	111.9	−33.8
	$CH_3O + H \rightarrow CH_3OH$	92.6	17.4

[a]The studies by Choi and Liu in ref [72]. [b]The studies by Neeti Kapur et al. in ref [75].

Second, starting from CH_3, Choi and Liu[72] have found that on Rh(111) surface, CH_4 formation by CH_3 hydrogenation is more favorable than CH_3CO formation by CO insertion into CH_3, which means that Rh catalyst has a better selectivity to CH_4 rather than C_2 oxygenates. In contrast, Mn-prompted MnCu catalyst exhibits a better selectivity for C_2 oxygenates rather than CH_4. In addition, the activation barrier of CHO insertion into CH_3 to CH_3CHO on MnCu catalyst is compatible and/or smaller than that on Rh catalyst.

Compared to Rh catalyst, above results show that introducing promoter Mn into Cu catalyst not only facilitate ethanol formation due to more CH_3 sources and less CH_3OH formation, but also effectively suppress CH_4 formation, as a result, the productivity and selectivity of ethanol can be well improved on MnCu catalyst.

3.8. General Discussions. On the pure Cu(211) surface,[14] CH_3 is very difficult to be formed due to the higher activation barrier compared to CH_3OH formation, as a result, less CH_3 sources can be received to join in CO insertion into CH_3 to CH_3CO, and then, CH_3CO is successively hydrogenated to ethanol. However, on the MnCu(211) surface, CH_3 formation is energetically compatible with CH_3OH formation. Moreover, the activation barrier of CH_3 formation is decreased, and the activation barrier of CH_3OH formation is significantly increased; thus, more CH_3 sources can be obtained to participate in CHO insertion into CH_3 to CH_3CHO, and CH_3CHO is successively hydrogenated to ethanol. Meanwhile, C_2 oxygenates formed via CHO insertion into CH_3 on MnCu(211) are more preferable both kinetically and thermodynamically than that on Cu(211). More importantly, compared with the traditional Rh catalyst,[72,75] more CH_3 sources can be obtained on the MnCu(211) surface, and CH_4 and CH_3OH formations can be effectively suppressed on MnCu(211) surface. Further, analyzing the reaction pathways on Cu(211) and MnCu(211) surfaces, introducing the Mn atom into Cu catalyst not only produces the new adsorption sites but also leads to the new formation pathway of CH_3 and C_2 oxygenates, suggesting that the promoter Mn at a step site of MnCu(211) surface can render the steps more active than Cu at a step site.

dx.doi.org/10.1021/jp409447u | J. Phys. Chem. C 2014, 118, 5243−5254

On the basis of analysis, we can obtain that by introducing promoter Mn into Cu catalyst, CH_3OH formation via CH_3O hydrogenation and CH_4 formation via CH_3 hydrogenation are minimized, and CH_3 sources via direct CH_3O dissociation and C_2 oxygenates via CHO insertion into CH_3 are maximized. As a result, the productivity and selectivity on MnCu(211) surface can be well improved compared those for to Cu(211) and Rh surfaces.

4. CONCLUSIONS

In this study, density functional theory calculations have been used to systematically investigate the mechanism of ethanol formation from syngas on the MnCu(211) surface, and to clarify the effect of promoter Mn into Cu-based catalysts. Our results suggest that CO + 3H → CHO + 2H → CH_2O + H → CH_3O is the initial step of CO hydrogenation. Starting from CH_3O, the most favorable monomer among all CH_x (x = 1−3) species, CH_3, is formed via direct CH_3O dissociation. CH_3OH is formed via CH_3O hydrogenation. Moreover, CH_3 formation is energetically compatible with CH_3OH formation. Further, starting from CH_3 species, CHO insertion into CH_3 to CH_3CHO is the most favorable pathway leading to C_2 oxygenates formation of ethanol precursor, and then CH_3CHO is hydrogenated to ethanol via CH_3CH_2O intermediates.

Compared to the Cu(211) surface, by introducing promoter Mn into Cu catalyst, CH_3 sources are maximized, and CH_3OH formation is minimized, and the C_2 oxygenates formation of ethanol precursor via CHO insertion into CH_3 is more favorable both in kinetics and thermodynamics. Meanwhile, the new adsorption sites for adsorbed species and new formation pathway of key intermediates (e.g., CH_3 and C_2 oxygenates of ethanol precursor) are presented. As a result, the productivity and selectivity of ethanol formation from syngas can be improved on MnCu catalyst, which means that Mn is a promising promoter for improved ethanol formation from syngas on Cu-based catalyst.

■ ASSOCIATED CONTENT

Supporting Information

The only one imaginary frequency corresponding to the transition state (Table S1) and the coordinates of all optimized structures (Table S2) involved in ethanol synthesis from syngas on MnCu(211) surface have been presented in detail. This material is available free of charge via the Internet at http://pubs.acs.org.

■ AUTHOR INFORMATION

Corresponding Author

*Tel.: +86 351 6018239. Fax: +86 351 6041237. E-mail: wangbaojun@tyut.edu.cn; quantumtyut@126.com.

Notes

The authors declare no competing financial interest.

■ ACKNOWLEDGMENTS

This work is financially supported by the National Natural Science Foundation of China (Nos. 21276003 and 21276171) and the National Natural Science Younger Foundation of China (Nos. 20906066 and 21103120). The authors are especially thankful for two anonymous reviewers for their helpful suggestions on the quality improvements of our present paper.

■ REFERENCES

(1) Pan, X.; Fan, Z.; Chen, W.; Ding, Y.; Luo, H.; Bao, X. Enhanced Ethanol Production Inside Carbon-Nanotube Reactors Containing Catalytic Particles. *Nat. Mater.* **2007**, *6*, 507−511.
(2) Henstra, A. M.; Sipma, J.; Rinzema, A.; Stams, A. J. M. Microbiology of Synthesis gas Fermentation for Biofuel Production. *Curr. Opin. Biotechnol.* **2007**, *18*, 200−206.
(3) Velu, S.; Satoh, N.; Gopinath, C. S.; Suzuki, K. Oxidative Reforming of Bio-ethanol over CuNiZnAl Mixed Oxide Catalysts for Hydrogen Production. *Catal. Lett.* **2002**, *82*, 145−152.
(4) Deluga, D. A.; Salge, J. R.; Schmidt, L. D.; Verykios, X. E. Renewable Hydrogen from Ethanol by Autothermal Reforming. *Science* **2004**, *303*, 993−997.
(5) Palsson, B. O.; Faith-Afshar, S.; Rudd, D. F.; Lightfoot, E. N. Biomass as a Source of Chemical Feedstocks: An Economic Evaluation. *Science* **1981**, *213*, 513−517.
(6) Ng, T. K.; Busche, R. M.; Mcdonald, C. C.; Hardy, R. W. F. Production of Feedstock Chemicals. *Science* **1983**, *219*, 733−740.
(7) Subramani, V.; Gangwal, S. K. A Review of Recent Literature to Search for an Efficient Catalytic Process for the Conversion of Syngas to Ethanol. *Energ. Fuel.* **2008**, *22*, 814−839.
(8) Burch, R.; Petch, M. I. Investigation of the Synthesis of Oxygenates from Carbon Monoxide/Hydrogen Mixtures on Supported Rhodium Catalysts. *Appl. Catal., A* **1992**, *88*, 39−60.
(9) Yin, H. M.; Ding, Y. J.; Luo, H. Y.; Zhu, H. J.; He, D. P.; Xiong, J. M.; Lin, L. W. Influence of Iron Promoter on Catalytic Properties of Rh-Mn-Li/SiO_2 for CO Hydrogenation. *Appl. Catal., A* **2003**, *243*, 155−164.
(10) Lu, Y. W.; Yu, F.; Hu, J.; Liu, J. Catalytic Conversion of Syngas to Mixed Alcohols over Zn-Mn Promoted Cu-Fe Based Catalyst. *Appl. Catal., A* **2012**, *429−430*, 48−58.
(11) Zhao, Y. H.; Yang, M. M.; Sun, D. P.; Su, H. Y.; Sun, K. J.; Ma, X. F.; Bao, X. H.; Li, W. X. Rh-Decorated Cu Alloy Catalyst for Improved C_2 Oxygenate Formation from Syngas. *J. Phys. Chem. C* **2011**, *115*, 18247−18256.
(12) Xu, R.; Wei, W.; Li, W. H.; Hu, T. D.; Sun, Y. H. Fe Modified $CuMnZrO_2$ Catalysts for Higher Alcohols Synthesis from Syngas: Effect of Calcination Temperature. *J. Mol. Catal. A* **2005**, *234*, 75−83.
(13) Boz, I.; Sahibzada, M.; Metcalfe, I. S. Kinetics of the Higher Alcohol Synthesis over a K-Promoted CuO/ZnO/Al_2O_3 Catalyst. *Ind. Eng. Chem. Res.* **1994**, *33*, 2021−2028.
(14) Zhang, R. G.; Wang, G. R.; Wang, B. J. Insights into the Mechanism of Ethanol Formation from Syngas on Cu and an Expanded Prediction of Improved Cu-based Catalyst. *J. Catal.* **2013**, *305*, 238−255.
(15) Wang, G. R.; Zhang, R. G.; Wang, B. J. Insight into the Preference Mechanism for C−C Chain Formation of C_2 Oxygenates and the Effect of Promoters in Syngas Conversion over Cu-based Catalysts. *Appl. Catal., A* **2013**, *466*, 77−89.
(16) Zhang, R. G.; Sun, X. C.; Wang, B. J. Insight into the Preference Mechanism of CH_x(x = 1−3) and C−C Chain Formation Involved in C_2 Oxygenate Formation from Syngas on the Cu(110) Surface. *J. Phys. Chem. C* **2013**, *117*, 6594−6606.
(17) Gupta, M.; Smith, M. L.; Spivey, J. Heterogeneous Catalytic Conversion of dry Syngas to Ethanol and Higher alcohols on Cu-Based Catalysts. *ACS Catal.* **2011**, *1*, 641−656.
(18) Slaa, J. C.; van Ommen, J. G.; Ross, J. R. H. The Synthesis of Higher Alcohols Using Modified Cu/ZnO/Al_2O_3 Catalysts. *Catal. Today* **1992**, *15*, 129−148.
(19) Xu, R.; Yang, C.; Wei, W.; Li, W. H.; Sun, Y. H.; Hu, T. D. Fe-Modified $CuMnZrO_2$ Catalysts for Higher Alcohols Synthesis from Syngas. *J. Mol. Catal. A* **2004**, *221*, 51−58.
(20) Gong, J.; Yue, H.; Zhao, Y.; Zhao, S.; Zhao, L.; Lv, J.; Wang, S.; Ma, X. Synthesis of Ethanol via Syngas on Cu/SiO_2 Catalysts with Balanced Cu^0-Cu^+ Sites. *J. Am. Chem. Soc.* **2012**, *134*, 13922−13925.
(21) Mahdavi, V.; Peyrovi, M. H.; Islami, M.; Mehr, J. Y. Synthesis of Higher Alcohols from Syngas over Cu-Co_2O_3/ZnO, Al_2O_3 Catalyst. *Appl. Catal., A* **2005**, *281*, 259−265.

(22) Sachtler, W. M. H.; Ichikawa, M. Catalytic Site Requirements for Elementary Steps in Syngas Conversion to Oxygenates over Promoted Rhodium. *J. Phys. Chem.* **1986**, *90*, 4752−4758.
(23) Bastein, A. G. T. M.; van Der Boogert, W. J.; van Der Lee, G.; Luo, H.; Schuller, B.; Ponec, V. Selectivity of Rh Catalysts in the Syngas Reactions. On the Role of Supports and Promoters. *Appl. Catal.* **1987**, *29*, 243−260.
(24) Chuang, S. C.; Goodwin, J. G., Jr; Wender, I. The Effect of Alkali Promotion on CO Hydrogenation over Rh/TiO_2. *J. Catal.* **1985**, *95*, 435−446.
(25) Kiennemann, A.; Breault, R.; Hindermann, J. P.; Laurin, M. Ethanol Promotion by the Addition of Cerium to Rhodium−Silica Catalysts. *J. Chem. Soc.* **1987**, *83*, 2119−2128.
(26) Luo, H. Y.; Zhang, W.; Zhou, H. W.; Huang, S. Y.; Lin, P. Z.; Ding, Y. J.; Lin, L. W. A Study of Rh-Sm-V/SiO_2 Catalysts for the Preparation of C_2-Oxygenates from Syngas. *Appl. Catal., A* **2001**, *214*, 161−166.
(27) Spivey, J. J.; Egbebi, A. Heterogeneous Catalytic Synthesis of Ethanol from Biomass-Derived Syngas. *Chem. Soc. Rev.* **2007**, *36*, 1514−1518.
(28) Ma, X. F.; Deng, H. Q.; Yang, M. M.; Li, W. X. Atomic and Molecular Adsorption on RhMn Alloy Surface: A First Principles study. *J. Chem. Phys.* **2008**, *129*, 244711−244718.
(29) Stroppa, A.; Mittendorfer, F.; Andersen, J. N.; Parteder, G.; Allegretti, F.; Srunev, S.; Netzer, E. P. Adsorption and Dissociation of CO on Bare and Ni-Decorated Stepped Rh(553) Surfaces. *J. Phys. Chem. C* **2009**, *113*, 942−949.
(30) Egbebi, A.; Schwartz, V.; Overbury, S. H.; Spivey, J. J. Effect of Li Promoter on Titania-Supported Rh Catalyst for Ethanol Formation from CO Hydrogenation. *Catal. Today* **2010**, *149*, 91−97.
(31) Haider, M. A.; Gogate, M. R.; Daivs, R. J. Fe-promotion of Supported Rh Catalysts for Direct Conversion of Syngas to Ethanol. *J. Catal.* **2009**, *261*, 9−16.
(32) Mo, X. H.; Gao, J.; Goodwin, J. G., Jr Role of Promoters on Rh/SiO_2 in CO Hydrogenation: A Comparison Using DRIFTS. *J. Catal.* **2009**, *147*, 139−149.
(33) Gao, J.; Mo, X. H.; Chien, A. C. Y.; Torres, W.; Goodwin, J. G., Jr CO Hydrogenation on Lanthana and Vanadia Doubly Promoted Rh/SiO_2 Catalysts. *J. Catal.* **2009**, *262*, 119−126.
(34) Mo, X. H.; Gao, J.; Umnajkaseam, N.; Goodwin, J. G., Jr; La, V. and Fe Promotion of Rh/SiO_2 for CO Hydrogenation: Effect on Adsorption and Reaction. *J. Catal.* **2009**, *267*, 167−176.
(35) Ma, X. F.; Su, H. Y.; Deng, H. Q.; Li, W. X. Carbon Monoxide Adsorption and Dissociation on Mn-Decorated Rh(111) and Rh(553) Surfaces: A First-Principles Study. *Catal. Today* **2011**, *160*, 228−233.
(36) Ojeda, M.; Granados, M. L.; Rojas, S.; Terreros, P.; Garcia-Garc, F. J.; Fierro, J. L. G. Manganese-Promoted Rh/Al_2O_3 for C_2-Oxygenates Synthesis from Syngas: Effect of Manganese Loading. *Appl. Catal., A* **2004**, *261*, 47−55.
(37) van Der Berg, F. G. A.; Glezer, J. H. E.; Sachtler, W. M. H. The Role of Promoters in CO/H_2 Reactions: Effects of MnO and MoO_2 in Silica-Supported Rhodium Catalysts. *J. Catal.* **1985**, *93*, 340−352.
(38) de Jong, K. P.; Glezer, J. H. E.; Kuipers, H. P. C. E.; Knoester, A.; Emeis, C. A. Highly Dispersed Rh/SiO_2 and $Rh/MnO/SiO_2$ Catalysts: 1. Synthesis, Characterization, and CO Hydrogenation Activity. *J. Catal.* **1990**, *124*, 520−529.
(39) Treviño, H.; Sachtler, W. M. H. On the Nature of Catalyst Promotion by Manganese in CO Hydrogenation to Oxygenates over RhMn/NaY. *Catal. Lett.* **1994**, *27*, 251−258.
(40) Ma, H. T.; Yuan, Z. Y.; Wang, Y.; Bao, X. H. Temperature-Programmed Surface Reaction Study on C_2-Oxygenate Synthesis over SiO_2 and Nanoporous Zeolitic Material Supported Rh−Mn Catalysts. *Surf. Interface Anal.* **2001**, *32*, 224−227.
(41) Mei, D. H.; Rousseau, R.; Kathmann, S. M.; Glezakou, V. A.; Engelhard, M. H.; Jiang, W. L.; Wang, C. M.; Gerber, M. A.; White, J. F.; Stevens, D. J. Ethanol Synthesis from Syngas over Rh-based/SiO_2 Catalysts: A Combined Experimental and Theoretical Modeling Study. *J. Catal.* **2010**, *271*, 325−342.
(42) Luo, H. Y.; Lin, P. Z.; Xie, S. B.; Zhou, H. W.; Xu, C. H.; Huang, S. Y.; Lin, L. W.; Liang, D. B.; Yin, P. L.; Xin, Q. The Role of Mn and Li Promoters in Supported Rhodium Catalysts in the Formation of Acetic Acid and Acetaldehyde. *J. Mol. Catal. A* **1997**, *122*, 115−123.
(43) Li, F. Y.; Jiang, D. E.; Zeng, X. C.; Chen, Z. F. Mn Monolayer Modified Rh for Syngas-to-Ethanol Conversion: A First-Principles Study. *Nanoscale* **2012**, *4*, 1123−1129.
(44) Ngo, H.; Liu, Y. Y.; Murata, K. Effect of Secondary Additives (Li, Mn) in Fe-Promoted Rh/TiO_2 Catalysts for the Synthesis of Ethanol from Syngas. *React. Kinet. Mech. Catal.* **2011**, *102*, 425−435.
(45) Ding, M. Y.; Qiu, M. H.; Wang, T. J.; Ma, L. L.; Wu, C. Z.; Liu, J. G. Effect of Iron Promoter on Structure and Performance of CuMnZnO Catalyst for Higher Alcohols Synthesis. *Appl. Energ.* **2012**, *97*, 543−547.
(46) Liu, Y. Y.; Murata, K.; Inaba, M.; Takahara, I.; Okabe, K. Mixed Alcohols Synthesis from Syngas over Cs- and Ni-Modified Cu/CeO_2 Catalysts. *Fuel* **2013**, *104*, 62−69.
(47) Delley, B. An All-Electron Numerical Method for Solving the Local Density Functional for Polyatomic Molecules. *J. Chem. Phys.* **1990**, *92*, 508−517.
(48) Delley, B. From Molecules to Solids with the $DMol^3$ Approach. *J. Chem. Phys.* **2000**, *113*, 7756−7764.
(49) Perdew, J. P.; Burke, K.; Ernzerhof, M. Generalized Gradient Approximation Made Simple. *Phys. Rev. Lett.* **1996**, *77*, 3865−3868.
(50) Perdew, J. P.; Wang, Y. Accurate and Simple Analytic Representation of the Electron-gas Correlation Energy. *Phys. Rev. B* **1992**, *45*, 13244−13249.
(51) Dolg, M.; Wedig, U.; Stoll, H.; Preuss, H. Energy-Adjusted ab Initio Pseudopotentials for the first row Transition Elements. *J. Chem. Phys.* **1987**, *86*, 866−872.
(52) Bergner, A.; Dolg, M.; Kuechle, W.; Stoll, H.; Preuss, H. Ab Initio Energy-Adjusted Pseudopotentials for Elements of Groups 13−17. *Mol. Phys.* **1993**, *80*, 1431−1441.
(53) Hohenberg, P.; Kohn, W. Inhomogeneous Electron Gas. *Phys. Rev. B* **1964**, *136*, B864−B871.
(54) Halgren, T. A.; Lipscomb, W. N. The Synchronous-Transit Method for Determining Reaction Pathways and Locating Molecular Transition States. *Chem. Phys. Lett.* **1977**, *49*, 225−232.
(55) Somorjai, G. A. *Introduction to Surface Chemistry and Catalysis*; Wiley and Sons: New York, 1994.
(56) Ponec, V. Alloy Catalysts: The Concepts. *Appl. Catal., A* **2001**, *222*, 31−45.
(57) Dahl, S.; Logadottir, A.; Egeberg, R. C.; Larsen, J. H.; Chorkendorff, I. Role of Steps in N_2 Activation on Ru(0001). *Phys. Rev. Lett.* **1999**, *83*, 1814−1817.
(58) Dahl, S.; Tornqvist, E.; Chorkendorff, I. Dissociative Adsorption of N_2 on Ru(0001): A Surface Reaction Totally Dominated by Steps. *J. Catal.* **2000**, *192*, 381−390.
(59) Klier, K.; Hess, J. S.; Herman, R. G. Structure Sensitivity of Methane Dissociation on Palladium Single Crystal surfaces. *J. Chem. Phys.* **1997**, *107*, 4033−4043.
(60) Uetsuka, H.; Watanabe, K.; Kimpara, K.; Kunimori, K. Structure Sensitivity in the Kinetics and the Dynamics of CO Oxidation over Stepped Pd(335) Studied by the Molecular Beam Infrared Chemiluminescence Technique: Determination of Working Site During the Steady-State Reaction. *Langmuir* **1999**, *15*, 5795−5799.
(61) Liu, Z. P.; Jenkins, S. J.; King, D. A. Step-Enhanced Selectivity of NO Reduction on Platinum-Group Metals. *J. Am. Chem. Soc.* **2003**, *125*, 14660−14661.
(62) Zambelli, T.; Wintterlin, J.; Trost, J.; Ertl, G. Identification of the "Active Sites" of a Surface-Catalyzed reaction. *Science* **1996**, *273*, 1688−1690.
(63) Xu, Y.; Mavrikakis, M. Adsorption and Dissociation of O_2 on Gold Surfaces: Effect of Steps and Strain. *J. Phys. Chem. B* **2003**, *107*, 9298−9307.
(64) Liu, Z. P.; Hu, P. General Rules for Predicting Where a Catalytic Reaction Should Occur on Metal Surfaces: A Density Functional Theory Study of C−H and C−O Bond Breaking/Making on Flat,

Stepped, Kinked Metal Surfaces. *J. Am. Chem. Soc.* **2003**, *125*, 1958−1967.
(65) Zhang, J.; Cao, X. M.; Hu, P.; Zhong, Z. Y.; Borgna, A.; Wu, P. Density Functional Theory Studies of Ethanol Decomposition on Rh(211). *J. Phys. Chem. C* **2011**, *115*, 22429−22437.
(66) Mavrikakis, M.; Bäumer, M.; Freund, H. J.; Nørskov, J. K. Structure Sensitivity of CO Dissociation on Rh Surfaces. *Catal. Lett.* **2002**, *81*, 153−156.
(67) Behrens, M.; Studt, F.; Kasatkin, I.; Kühl, S.; Hävecker, M.; Abild-Pedersen, F.; Zander, S.; Girgsdies, F.; Kurr, P.; Kniep, B. L.; Tovar, M.; Fischer, R. W.; Nørskov, J. K.; Schlögl, R. The Active Site of Methanol Synthesis Over $Cu/ZnO/Al_2O_3$ Industrial Catalysts. *Science* **2012**, *336*, 893−897.
(68) Bihlmayer, G.; Kurz, Ph.; Blügel, S. Overlayers, Interlayers, and Surface Alloys of Mn on the Cu(111) Surface. *Phy. Rev. B* **2000**, *62*, 4726−4732.
(69) Flores, T.; Hansen, M.; Wuttig, M. Structure and Growth of Mn on Cu(100). *Surf. Sci.* **1992**, *279*, 251−264.
(70) D'Addato, S.; Finetti, P. An Extended X-ray Absorption Fine Structure Study of Mn Ultrathin Films Grown on Cu(100). *Surf. Sci.* **2001**, *471*, 203−208.
(71) Pan, W.; Popescu, R.; Meyerheim, H. L.; Sander, D.; Robach, O.; Ferrer, S.; Lin, M. T.; Kirschner, J. Stress and Structure of $c(2 \times 2)$ and p2gg MnCu(001) Surface Alloy. *Phys. Rev. B* **2005**, *71*, 174439−1−7.
(72) Choi, Y. M.; Liu, P. Mechanism of Ethanol Synthesis from Syngas on Rh(111). *J. Am. Chem. Soc.* **2009**, *131*, 13054−13061.
(73) Campana, L.; Selloni, A.; Weber, J.; Goursot, A. Cation Siting and Dynamical Properties of Zeolite Offretite from First-Principles Molecular Dynamics. *J. Phys. Chem. B* **1997**, *101*, 9932−9939.
(74) Chen, Q. L.; Tang, C. Q.; Zheng, G. First-Principles Study of TiO_2 Anatase(101) Surfaces Doped with N. *Phys. B: Condensed. Matter.* **2009**, *404*, 1074−1078.
(75) Kapur, N.; Hyun, J.; Shan, B.; Nicholas, J. B.; Cho, K. Ab Initio Study of CO Hydrogenation to Oxygenates on Reduced Rh Terraces and Stepped Surfaces. *J. Phys. Chem. C* **2010**, *114*, 10171−10182.
(76) Grabow, L. C.; Mavrikakis, M. Mechanism of Methanol Synthesis on Cu through CO_2 and CO Hydrogenation. *ACS Catal.* **2011**, *1*, 365−384.
(77) Studta, F.; Abild-Pedersena, F.; Wu, Q. X.; Jensen, A. D.; Temel, B.; Grunwaldte, J. D.; Nørskova, J. K. CO hydrogenation to methanol on Cu−Ni catalysts: Theory and experiment. *J. Catal.* **2012**, *293*, 51−60.
(78) Zhao, Y. H.; Sun, K. J.; Ma, X. F.; Liu, J. X.; Sun, D. P.; Su, H. Y.; Li, W. X. Carbon Chain Growth by Formyl Insertion on Rhodium and Cobalt Catalysts in Syngas Conversion. *Angew. Chem., Int. Ed.* **2011**, *50*, 5335−5338.
(79) Deluzarche, A.; Hindermann, J. P.; Kieffer, R.; Breault, R.; Kiennernann, A. Ethanol Formation Mechanism from $CO+H_2$ on a Rh/TiO_2 Catalyst. *J. Phys. Chem.* **1984**, *88*, 4993−4995.
(80) Slaa, J. C.; van Ommen, J. G.; Ross, J. R. H. The Synthesis of Alcohols Using $Cu/ZnO/Al_2O_3$+(Ce or Mn) Catalysts. *Catal. Today* **1995**, *2*, 79−89.
(81) Pan, W. X.; Cao, R.; Griffin, G. L. Direct Alcohol Synthesis Using Copper/Cobalt Catalysts. *J. Catal.* **1988**, *114*, 447−456.
(82) Nunan, J. G.; Herman, R. G.; Klier, K. Higher Alcohol and Oxygenate Synthesis over $Cs/Cu/ZnO/M_2O_3$(M Al, Cr) Catalysts. *J. Catal.* **1989**, *116*, 222−229.